The Mechanism of Acetyl-CoA Synthase Through the Lens of a Nickel Model System

Authors: Shounak Nath,[1] Leonel Griego,[1] and Liviu M. Mirica[1,*]

Affiliations:

[1] Department of Chemistry, Beckman Institute for Advanced Science and Technology, Carle Illinois College of Medicine, The Neuroscience Program, Department of Bioengineering, Carle Woese Institute for Genomic Biology, University of Illinois Urbana-Champaign, Urbana, Illinois, 61801.

* Corresponding author. Email: mirica@illinois.edu

ABSTRACT

Given the urgent need to develop new methods of CO_2/CO utilization, understanding the mechanism of acetyl-CoA synthase (ACS) – a primordial nickel enzyme that converts these gases into a source of cellular energy, is crucial; however, conflicting hypotheses and a dearth of well-characterized bioorganometallic intermediates have hindered a proper understanding of its mechanism. Herein, we report a functional model system that supports several organometallic intermediates proposed for ACS, including the long sought-after Ni(methyl)(CO) species, and promotes all key reaction steps during catalysis: methylation, carbonylation, and thiolysis. Our investigations provide key mechanistic insights that are directly relevant to ACS, suggesting that binding of a second CO molecule to the Ni center promotes migratory insertion, that one-electron oxidation of Ni drives a fast reductive elimination, that both paramagnetic and diamagnetic Ni intermediates are involved, and confirm the feasibility of a random binding order of the methyl and CO groups to the Ni center.

INTRODUCTION

The microbial nickel enzyme acetyl-CoA synthase (ACS) constitutes a pivotal component of the Wood-Ljungdahl Pathway (WLP), and together with carbon monoxide dehydrogenase (CODH) fixes atmospheric CO_2/CO into the global carbon cycle.[1-5] In the present context of the ever-increasing imbalance of these gases in the atmosphere, an in-depth understanding of this enzyme pathway is essential to devise new strategies for CO_2/CO fixation into synthetically useful chemicals.[6] Specifically, the mechanism of ACS has parallels to the industrial Monsanto and Cativa processes for acetic acid synthesis, albeit they operate under harsh conditions and employ precious Rh and Ir catalysts.[7,8] ACS catalyzes the synthesis of acetyl-CoA in the final step of the WLP through the condensation of CO (supplied from CODH via a gas channel), a methyl group (transferred from the methylcobalamin of a corrinoid iron-sulfur protein), and coenzyme A *via* several organometallic Ni intermediates (Fig. 1a). In certain microbes, the WLP can operate in the reverse direction, wherein acetyl-CoA is metabolized into CO_2 and methane. The first step in this process is carried out by a related Ni enzyme acetyl-CoA decarbonylase/synthase (ACDS) that reversibly cleaves the acetate C-C bond via a Ni-based decarbonylation reaction.[9,10] The A cluster in the active site of ACS consists of a thiolate bridged Ni_p-Ni_d dinuclear cluster, yet it commonly accepted that only the 3-coordinate proximal Ni_p center is the site of substrate binding (Fig. 1d).[11] Nevertheless, conflicting hypotheses and a dearth of well-characterized bioorganometallic intermediates have hindered a proper understanding of the mechanism of ACS. A Ni(methyl)(CO) intermediate, which has both the methyl and CO groups directly bound to the Ni center, has been proposed to be involved in the enzyme mechanism,[12] yet it has never been observed.[13] This conundrum is exacerbated by the fact that no such intermediate has been isolated in any synthetic model of ACS.[14-17] Due to the presence of a CO alcove near the active site, and with the recent discovery of a two-CO bound state at the Ni_p center,[18,19] the role of excess CO on the mechanism

of ACS is also not well understood. In addition, although it is known that the enzyme needs a reductive activation from its inactive Ni^{II} state to enter the catalytic cycle,[20] the precise oxidation states of the catalytically relevant intermediates is ambiguous.[1,5,21] Finally, the order of binding of the methyl and CO groups to the Ni center, whether ordered or random, has also been debated (Fig. 1a).[22]

Synthetic models that mimic the structure and/or the function of ACS are useful to establish molecular principles governing its mechanism. Several organometallic Ni complexes have been developed over the years as models for ACS (Fig. 1b), however they only showcase a limited set of the proposed enzymatic catalytic steps (Fig. 1c).[14-16,23-28] Recently, Shafaat and coworkers have reported a modified azurin protein containing a mononuclear 3-coordinate Ni center as a model for ACS that provided insights into the nature of several proposed organometallic intermediates.[17,29-31]

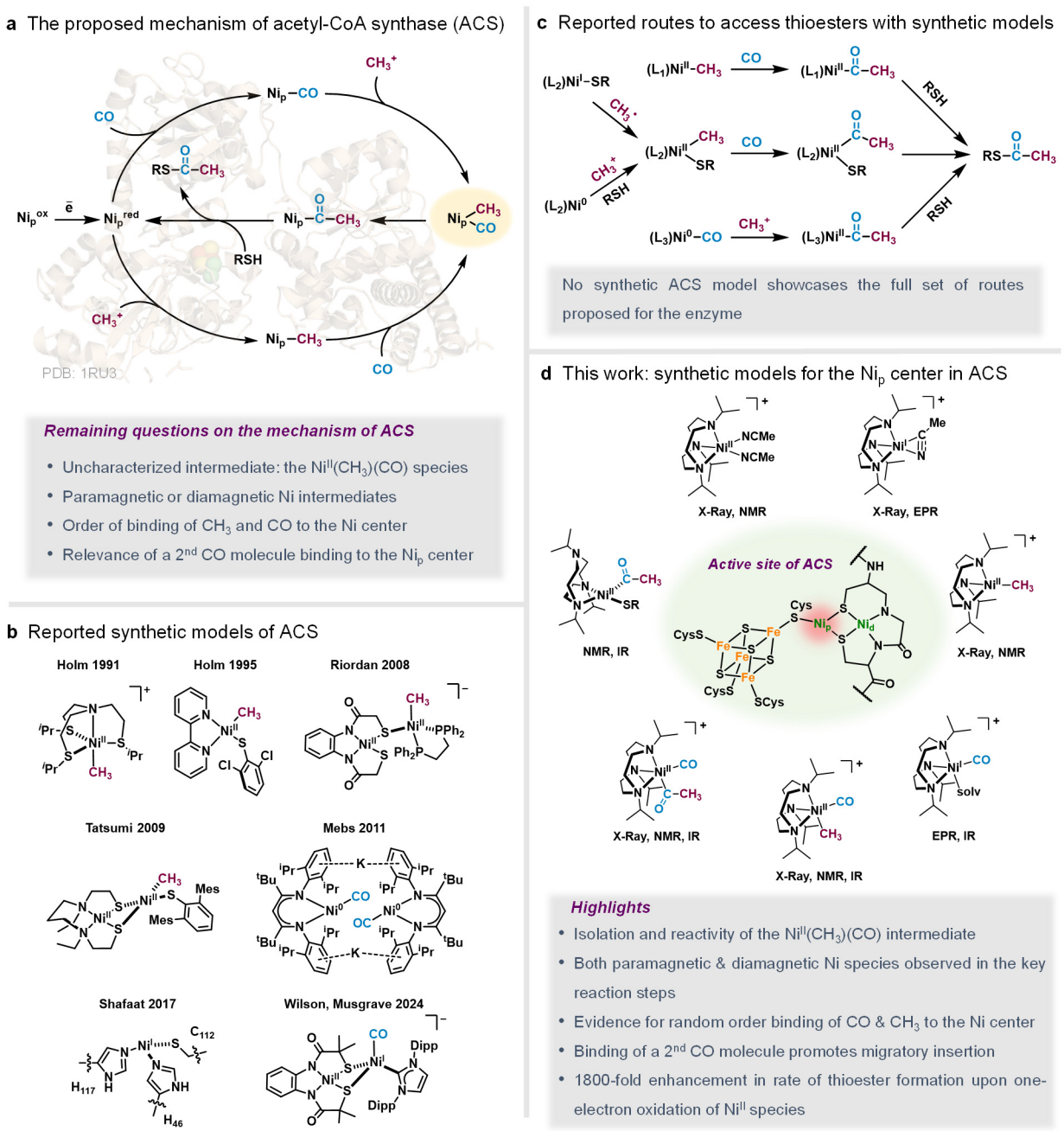

Fig. 1. Acetyl-CoA Synthase and models. (a) The proposed mechanism for acetyl-CoA synthase (ACS) showing substrate binding at the proximal Ni_p site. Ni intermediates involved can either be paramagnetic (Ni^I/Ni^{III}) or diamagnetic (Ni^0/Ni^{II}). The two possible substrate binding routes are shown: CO binding followed by methyl (top pathway) and methyl binding followed by CO (bottom pathway) The crystal structure of the monomeric form of ACS obtained from *Carboxydothermus Hydrogenoformans* (PDB: 1RU3) is shown in the background; **(b)** Reported

functional models of ACS that promote formation of thioesters; **(c)** Synthetic routes to access thioesters with the reported synthetic functional models of ACS; **(d)** Present work: mononuclear functional models for the Ni_p site of ACS.

Herein, we report a comprehensive study of a synthetic functional mimic of ACS that enables the exploration of all organometallic intermediates proposed for the catalytic steps involved in the ACS mechanism. A series of Ni complexes supported by the tridentate macrocyclic ligand 1,4,7-triisopropyl-1,4,7-triazacyclononane (^{i}Pr$_3$tacn) have been synthesized and their organometallic reactivity was investigated in detail (Fig. 1d). Importantly, the key Ni^{II}(methyl)(CO) intermediate has been isolated for the first time. In addition, our investigations provide key mechanistic insights that are directly relevant to mechanism of ACS: the importance of a second CO molecule binding to the Ni center to drive the CO migratory insertion step, the relevance of both diamagnetic and paramagnetic Ni intermediates during the catalytic steps, and the feasibility of a random binding order of the methyl and CO groups to the Ni center. Finally, we show that the reductive elimination of the thioester product from an organometallic Ni^{II} species is ~1800 times faster upon one-electron oxidation, thus likely proceeding via a Ni^{III} intermediate. Importantly, the mechanistic studies described herein could be adapted to probe the mechanistic details of the ACS/ACDS enzymes.

RESULTS AND DISCUSSION

A synthetic model for the methylated state of ACS

The previously reported bis-solvento Ni complex [(^{i}Pr$_3$tacn)Ni^{II}(NCMe)$_2$](PF$_6$)$_2$ (**1**) was chosen to model the solvent-bound inactive oxidized state (A_{ox}) of ACS.[32] Its Ni^{II}/Ni^{I} redox couple

(-1.20 V vs Fc^+/Fc, -0.56 V vs NHE) compares well to that of the experimentally estimated redox potential for ACS (-0.50 to -0.54 V vs NHE)[33] or its computed value (-0.67 V vs NHE),[34] as well as that of the Ni-substituted azurin model of ACS.[29] This implies a similarity in the electronic environment around the Ni center between this model complex and the biological system. Accordingly, the one-electron reduction of **1** generates the Ni^I complex [(^{i}Pr$_3$tacn)Ni^I(η^2-NCMe)]PF_6 (**2**) that models the reduced catalytically active state (A_{red}) of ACS.[35]

As a model for the methylated state (A_{Me}) of ACS, the Ni^{II}-monomethyl complex [(^{i}Pr$_3$tacn)Ni^{II}(CH_3)]PF_6 (**3**) was synthesized as a purple solid in 82% yield via a transmetallation reaction of **1** with a stoichiometric amount of DABAL-Me_3[36] (Fig. 2a). An effective magnetic moment of 2.88 μ_B in MeCN was obtained for **1**, which supports a high spin (S=1) Ni^{II} center. The solid-state structure revealed a distorted tetrahedral coordination environment (τ_4 = 0.64) at the Ni center (Fig. 2b, i). Notably, tetrahedral high spin organometallic Ni^{II} complexes are difficult to access, particularly because the strong field σ-donor characteristics of the alkyl group favors spin pairing.[24,30,37] Although the A_{Me} state observed in ACS is low spin,[13] Shafaat and coworkers showed that a Ni-substituted (M121A)Azurin can replicate all the proposed steps of ACS from a high spin tetrahedral Ni^{II} (CH_3) complex.[17] Interestingly, **3** could also be generated in 26% yield via a methyl transfer to the Ni^I complex from the methylcobaloxime Co^{III}(dmgBF_2)$_2$(CH_3)(py) in the presence of cobaltocene ($CoCp_2$) as an external reductant. This reaction directly models the methyl transfer step by the methylcobalamin to the reduced Ni_p state of ACS.[1,38]

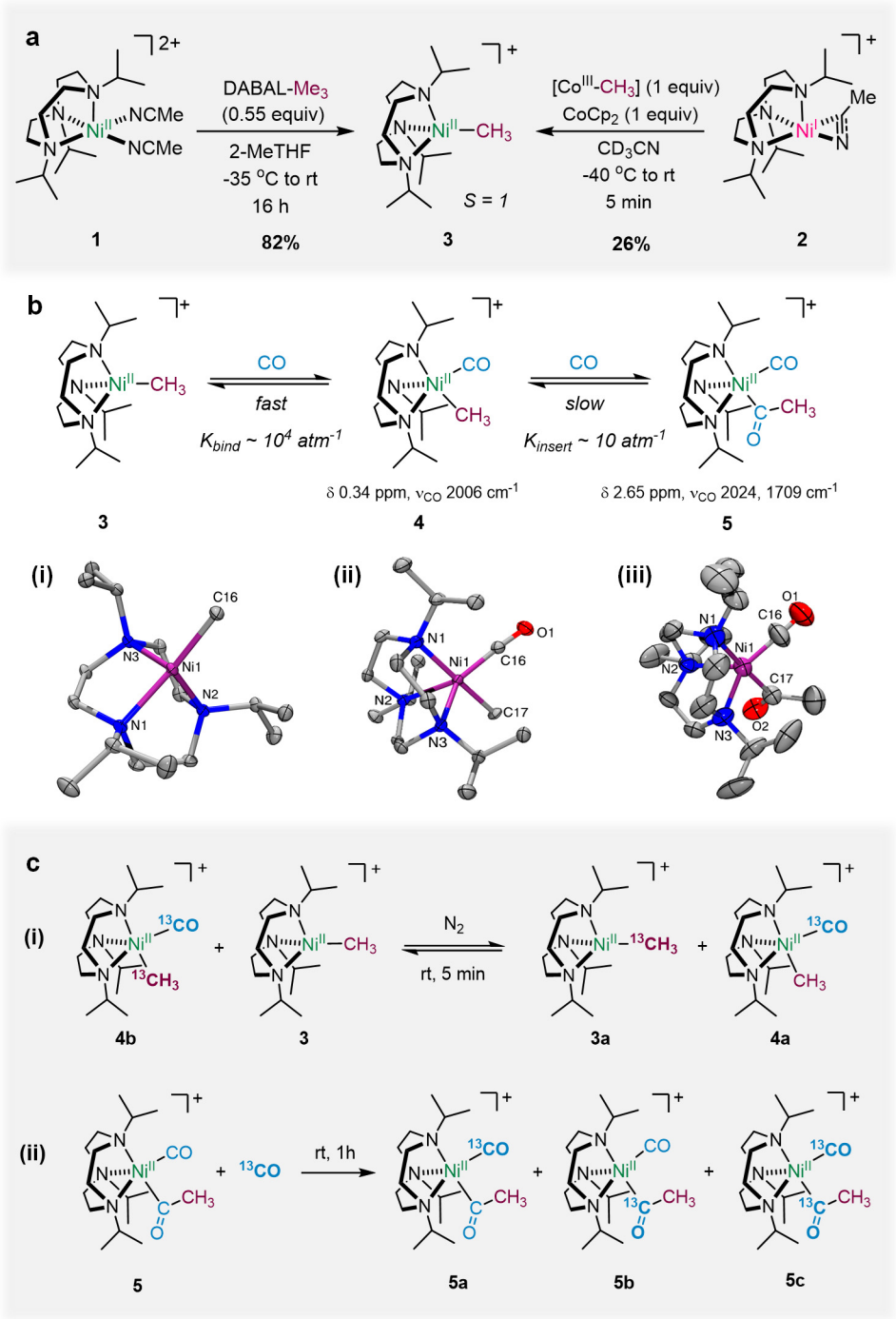

Fig. 2. Synthesis of models of the methylated state of ACS and its CO reactivity. (a) Synthesis of the Ni-monomethyl complex (**3**) as a model for the methylated state of ACS. DABAL-Me_3: bis(trimethylaluminium)-1,4-diazabicyclo[2.2.2]octane; [Co^{III}-CH_3]: $Co^{III}(dmgBF_2)_2(CH_3)(py)$ (dmg = dimethylglyoxime, py = pyridine); $CoCp_2$: cobaltocene. **(b)** The two-step reaction of **3**

with CO, to access complexes **4** and **5**. (i-iii) ORTEP representations with ellipsoids drawn at 50% probability for (i) **3**, selected bond lengths (Å): Ni1–N1, 2.066(3); Ni1–N2, 2.075(3); Ni1–N3, 2.053(3); Ni1–C16, 1.988(3); (ii) **4**, selected bond lengths (Å): Ni1–N1, 2.036 (5); Ni1–N2, 2.126(5); Ni1–N3, 2.143(5); Ni1–C16, 1.730(6); Ni1–C17, 1.992(6); C16–O1, 1.140(8); (iii) **5**, selected bond lengths (Å): Ni1–N1, 2.092 (5); Ni1–N2, 2.166(5); Ni1–N3, 2.078(5); Ni1–C16, 1.761(9); Ni1–C17, 1.974(7); C16–O1, 1.158(11); C17–O2, 1.201(8). Hydrogen atoms, anions, and non-coordinated solvent molecules were omitted for clarity. **(c)** ^{13}C labelling experiments demonstrating the reversibility of (i) CO binding and (ii) migratory insertion reactions.

As a result of its distorted tetrahedral geometry, **3** exhibits an accessible coordination site, and upon exposure to 1 atm CO in CH_2Cl_2 undergoes an immediate color change from purple to orange. The ^1H NMR of this reaction mixture shows a paramagnetic-to-diamagnetic spectral change that displays a singlet peak at δ 0.34 ppm, assigned to Ni-CH_3 group, and continued exposure to CO leads to formation of a new singlet peak at δ 2.65 ppm, assigned to a Ni^{II}- $COCH_3$ group, that forms with the concomitant decay of the initial Ni^{II}-CH_3 peak (Figs. S31-S32). In addition, *in situ* monitoring by FT-IR reveals an immediate appearance of a peak at ~2000 cm^{-1} (assigned to the CO stretch of a Ni^{II}-CO species), which persists throughout the reaction and is accompanied by a subsequent growth of a peak at ~1700 cm^{-1}, assigned to the CO stretch of a Ni^{II}-$COCH_3$ species (Figs. S35-S36). Overall, these observations are in support of a two-step reaction of **3** with CO: an initial rapid binding of CO to the vacant coordination site, followed by a slow migratory insertion of CO into the Ni^{II}-CH_3 bond to form a Ni^{II}-$COCH_3$ species (Fig. 2b). Gratifyingly, exposing **3** to 1 atm CO at low temperature enabled the isolation of a rare complex $[(^iPr_3tacn)Ni^{II}(CH_3)(CO)]PF_6$ (**4**) as an orange, diamagnetic solid in 90% yield, and single crystal X-ray diffraction analysis reveals a trigonal bipyramidal geometry at the Ni center (Fig. 2b, ii). To

the best of our knowledge, this is the first isolated Ni(methyl)(CO) complex as an intermediate in the CO migratory insertion of a Ni-methyl complex that models the elusive Ni(methyl)(CO) intermediate in ACS.[39,40] Finally, prolonged exposure of a THF solution of **3** to 1 atm CO at room temperature followed by vapor diffusion of pentane led to the isolation of orange crystals of [(^{i}Pr$_3$tacn)Ni^{II}(COCH$_3$)(CO)]PF$_6$ (**5**), with the X-ray structure revealing a distorted square pyramidal geometry at the Ni center and confirming the formation of an Ni(acetyl)(CO) species (Fig. 2b, iii).

In ACS, acetyl-CoA formation is known to proceed via a reversible CO binding/migratory insertion at the Ni center, while ACDS is known to reversibly cleave the C-C bond of acetate *via* formation of acetyl-CoA, followed by a metal-based decarbonylation reaction. In this context, crossover/exchange studies were carried out with isotopically labelled complexes, and addition of **3** to a solution of [(^{i}Pr$_3$tacn)Ni^{II}(^{13}CH$_3$)(^{13}CO)]PF$_6$ (**4b**) in CD$_2$Cl$_2$ under N$_2$ led to the formation of the mono-labelled species [(^{i}Pr$_3$tacn)Ni^{II}(^{12}CH$_3$)(^{13}CO)]PF$_6$ (**4a**) (Figs. 2c, i, and S46), suggesting that the CO molecule can "hop" from one Ni^{II}-Me complex to another and thus supporting a reversible initial CO binding to **3**. UV-vis titration experiments reveal a large equilibrium constant of ~10^4 atm^{-1} for the CO binding to **3** (Figs. S18-S19). Introduction of ^{13}CO to a solution of **5** in CD$_2$Cl$_2$ led to ^{13}C enrichment at the Ni-bound CO position, but also at the carbonyl carbon of the acetyl group, all three complexes **5a**, **5b**, and **5c** being detected by ^{13}C NMR (Figs. 2c, ii and S48). This exchange of the acetyl carbonyl with free CO provides strong evidence that the migratory insertion of CO into the Ni^{II}-CH$_3$ bond in **4** is also reversible. Additional support for the reversibility of migratory insertion was obtained from ^{1}H NMR, wherein it was observed that under static vacuum a solution of **5** slowly converts to **4** (Fig. S34).

The CO migratory insertion has been shown to be the rate determining step of the entire catalytic process in ACS.[41] A recent discovery of a CO alcove near the active site of ACS

presumably allows for CO saturation conditions during migratory insertion.[42] This is particularly relevant given the recent spectroscopic identification of two CO molecules bound to the Ni_p site.[19] In this context, it was observed that **4** undergoes migratory insertion only in the presence of excess CO. Monitoring by UV-vis of the conversion of **4** to **5** under 1 atm CO reveals a first-order growth of an absorption peak at 340 nm, corresponding to the near complete formation (>95%) of the Ni-acetyl complex **5** (Fig. S33), along with a concomitant decay of the absorption peak at 253 nm (Fig. 3a, i). A rate constant k_{obs} of 1.26 ± 0.01 x 10^{-3} s^{-1} could be extracted for this process at room temperature, and k_{obs} was found to increase linearly with an increase in CO concentration (Fig. 3b, i). This supports a reaction that is first order in CO and indicates an associative binding of CO occurring at or before the rate determining step. An Eyring analysis of this process at various temperatures yields the following activation parameters: $\Delta H^{\ddagger}$ = 9 ± 1 kcal/mol and $\Delta S^{\ddagger}$ = -41 ± 2 cal/mol K (Fig. 3b, ii), and a free energy of activation $\Delta G^{\ddagger}$ = 21 ± 1 kcal/mol (298 K, 1 atm CO). Importantly, the large negative value for $\Delta S^{\ddagger}$ further supports an associative mechanism for the CO migratory insertion step.

A solution of **5** is stable only under 1 atm CO and slowly converts to **4** when CO is removed from the headspace of the reaction vessel. The kinetics of this process was followed via UV-vis to reveal a slow first order decay in the peak at 340 nm and a concomitant increase in the peak at 253 nm (Fig. 3a, ii), corresponding to a rate constant for the deinsertion of CO from **5** of 2.03 ± 0.02 x 10^{-4} s^{-1}, the CO deinsertion step thus being an order of magnitude slower than the reverse CO migratory insertion. More mechanistic insights were obtained from ^{13}CO labelling experiments wherein it was observed that the introduction of ^{13}CO to a solution of **4** led to the incorporation of CO at all possible sites of the $Ni^{II}(COCH_3)(CO)$ complex (**5a**, **5b**. and **5c**, Fig. S47). This rules out (a) a direct insertion of the incoming CO into the Ni^{II}-CH_3 bond and (b) a zero-order process involving an initial CO migratory insertion followed by CO binding, as these two pathways would

exclusively lead to the formation of **5b** and **5a**, respectively. Furthermore, the relative fractions of **5a** and **5b** stay nearly equal throughout the reaction (Figs. S49-S51), implying that **5a** and **5b** should arise from a common intermediate. These results are suggestive of an initial binding of CO to the Ni center in **4** to form a transient $[LNi^{II}(CH_3)(CO)_2]^+$ species, prior to one of the two CO groups migrating into the Ni-methyl bond (Fig. 3c). This is consistent with the large negative value of $\Delta S^{\ddagger}$ obtained from the Eyring analysis, and also parallels the CO migratory insertion for a phosphine-Ni^{II} complex proposed to operate via a five-coordinate intermediate formed upon coordination of a second CO molecule to the Ni center prior to migratory insertion.[39] Modelling the conversion of **4** to **5** by a two-step reversible process enables the determination of the equilibrium constant for the CO migratory insertion to be 11.9 ± 5.3 atm^{-1} (pages S70-S71), which is three orders of magnitude lower than the equilibrium constant measured for the CO binding to **3** (Fig. 2b). Overall, the equilibrium constant for the conversion of **3** to **5** is determined to be ~10^5 atm^{-2}, which is similar to the equilibrium constant of 10^4 atm^{-1} estimated for ACS.[41]

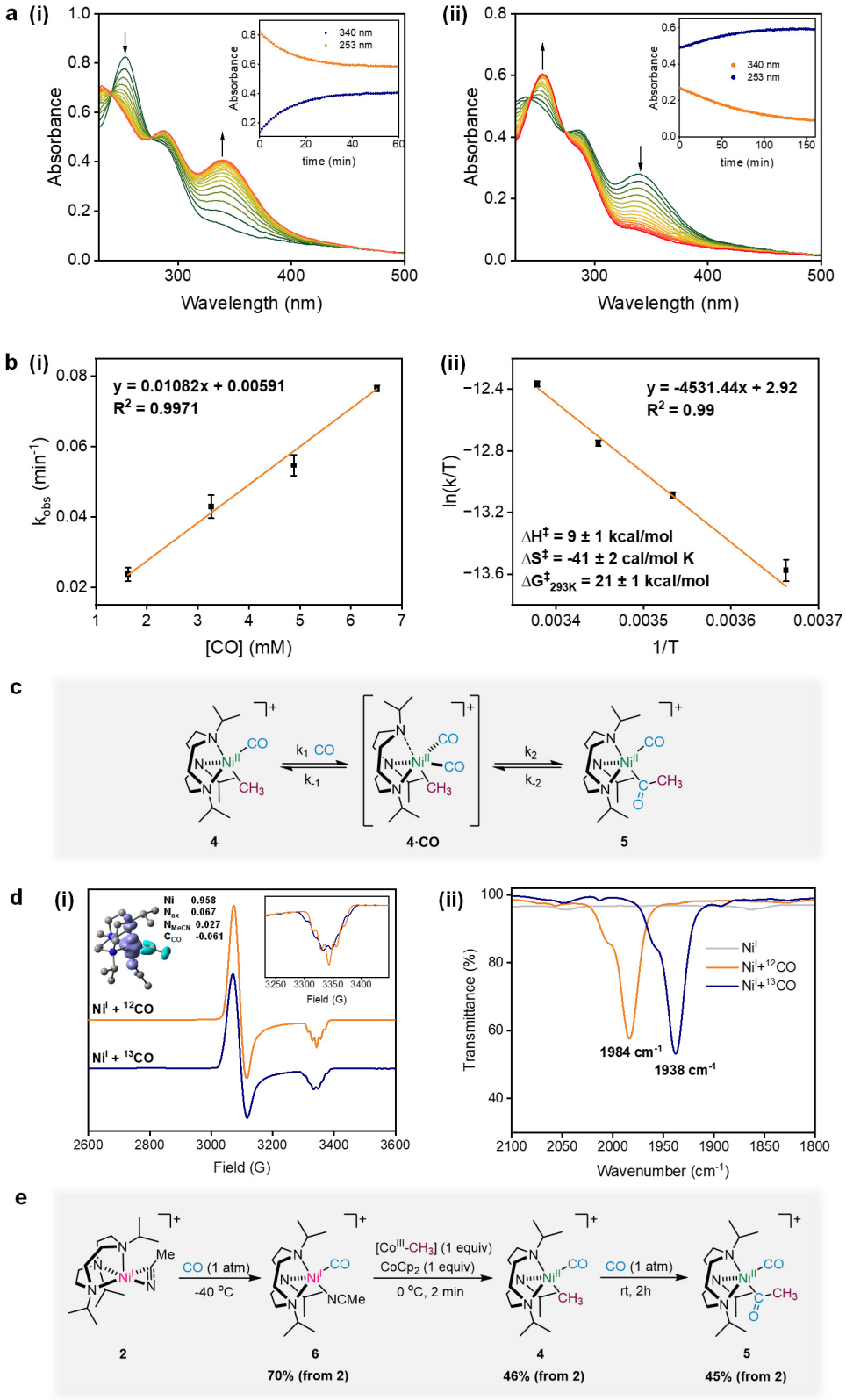

Fig. 3. CO migratory insertion and the Ni^{I}(CO) complex supported by ^{i}Pr$_3$tacn. (a) UV-vis profile for (i) the reaction of **4** with 1 atm CO to form **5** and (ii) for the conversion of **5** to **4** under

1 atm N_2. **(b)** Kinetics studies for the migratory CO insertion step: (i) [CO] dependence on k_{obs}, first-order dependence on [CO] observed; (ii) Eyring plot for the CO migratory insertion for the evaluation of activation parameters. **(c)** Proposed mechanism for the CO migratory insertion. **(d)** Spectroscopic characterization of the Ni^{I}(CO) complex supported by $^{i}Pr_3$tacn: (i) X-band EPR spectra obtained upon exposure **2** to 1 atm ^{12}CO or ^{13}CO at -78˚C, recorded at 77 K in 3:1 PrCN/MeCN. Inset shows the spin density plot drawn at a 0.0025 isovalue; (ii) Solution IR spectra obtained upon exposure of **2** to 1 atm ^{12}CO or ^{13}CO. Spectra recorded in a solution of MeCN/PrCN (1:3). **(e)** Methylation of the *in situ* generated [($^{i}Pr_3$tacn)Ni^{I}(CO)(NCMe)]$^{+}$ complex **6** with the methylcobaloxime in the presence of an external reductant.

A synthetic model for the carbonylated Ni^{I} state of ACS

The Ni^{I}(CO) intermediate, A_{NiFeC}, is the most well characterized state in ACS,[43,44] however, there have been questions regarding its involvement in the enzyme catalytic cycle.[45,46] In an attempt to model this species, exposure of the Ni^{I} complex **2** to 1 atm CO at -78 ˚C led to an immediate change in the EPR spectrum to yield an axial signal with $g_x = g_y = 2.183$ and $g_z = 2.015$, along with superhyperfine coupling to two N atoms in the g_z direction ($A_{2N} = 14$ G, Figs. 3d, i and S55). Use of ^{13}CO instead of ^{12}CO led to the appearance of additional coupling in the g_z direction from the ^{13}C (I = ½) nucleus ($A_C = 14$ G), thus confirming the formation of a Ni^{I}(CO) intermediate. Density functional theory (DFT) calculations reproduce the pseudo-axial g tensor and the superhyperfine coupling constants of the putative MeCN-bound [($^{i}Pr_3$tacn)Ni^{I}(CO)(NCMe)]$^{+}$ complex **6** (Tables S21-S22), and the spin density plot reveals that the unpaired electron resides mainly on the Ni d_{z^2} orbital, with significant contributions from the axial N atom of $^{i}Pr_3$tacn, the acetonitrile molecule, and the coordinated CO (Fig 3d, i, inset). Notably, a five-coordinate Ni^{I}-

isocyanide complex supported by the same ligand framework has been reported recently,[32] suggesting that such five-coordinate Ni^{I} complexes with suitable π acceptors can be stabilized with $^{i}Pr_3tacn$. Further confirmation for the formation of a $Ni^{I}(CO)$ species was obtained from FT-IR, which reveals a CO stretch at 1984 cm^{-1} that red-shifts to 1938 cm^{-1} when ^{13}CO is used (Fig. 3d, ii). This shift is consistent with a molecule of CO bound to Ni, as confirmed by DFT calculations (Fig. S95); the extent of CO activation achieved in this model system is comparable to the $Ni^{I}(CO)$ state in ACS (ν_{CO} = 1996 cm^{-1}),[47] and also to that in the $Ni^{I}(CO)$ azurin model of ACS (ν_{CO} = 1976 cm^{-1}).[29]

Importantly, the $Ni^{I}(CO)$ species **6** is competent for methylation with the methylcobaloxime $Co^{III}(dmgBF_2)_2(CH_3)(py)$ in presence of $CoCp_2$ as the reductant, with complex **4** being formed in 46% yield and subsequently leading to formation of **5** upon continued exposure to CO (Fig. 3e). Overall, these results suggest the intermediacy of the same $Ni^{II}(CH_3)(CO)$ species **4**, irrespective of the order of addition of CO and CH_3 to the Ni center, and provide strong support for the proposed random binding order of CO and CH_3 to the ACS active site.[22]

Thiolysis of the synthetic models of ACS

In ACS there is no unambiguous evidence of how CoA binds to the Ni center to promote acetyl-CoA formation.[1,48] To probe this aspect, complex [($^{i}Pr_3tacn$)$Ni^{II}(CH_3)$(SPh)] (**7**) was synthesized from **3**, using thiophenolate as a model for CoA. Upon exposure of **7** to 1 atm CO at -78˚C, spectroscopic signatures corresponding to a Ni-bound acetyl group were observed (^{1}H NMR: δ 2.12 ppm, and IR: ν_{CO} 1628 cm^{-1}), consistent with the formation of the [($^{i}Pr_3tacn$)Ni^{II}(acetyl)(SPh)] complex (**8**, Fig. 4a).[23,26,49] Warming up the above solution to room temperature led to the disappearance of the Ni-acetyl peak and concomitant formation of S-phenyl thioacetate in 77% yield.

Since CoA is proposed to be the final substrate in the catalytic cycle of ACS,[22] a more faithful synthetic route was employed in which **4** was reacted with PhSNa in THF-d_8 at -78˚C in the absence of excess CO (Fig. 4b, top), leading to the formation of the same species **8**, as shown by ^{1}H NMR and FT-IR, and eventual formation of S-phenyl thioacetate in 48% yield at room temperature; this reactivity suggests thiolates behave in a manner similar to CO by driving the CO migratory insertion step. Moreover, the yield of the thioacetate product increases to 77% in the presence of 1 atm CO (Fig. 4b, condition b), and this trend is conserved across a range of aryl and alkyl thiolates with varying electronic and steric preferences (Fig. 4b). Finally, thiolysis of complex **5** with either aryl or alkyl thiolates also leads to the formation of thioesters in high yields (Fig. 4b, condition c).

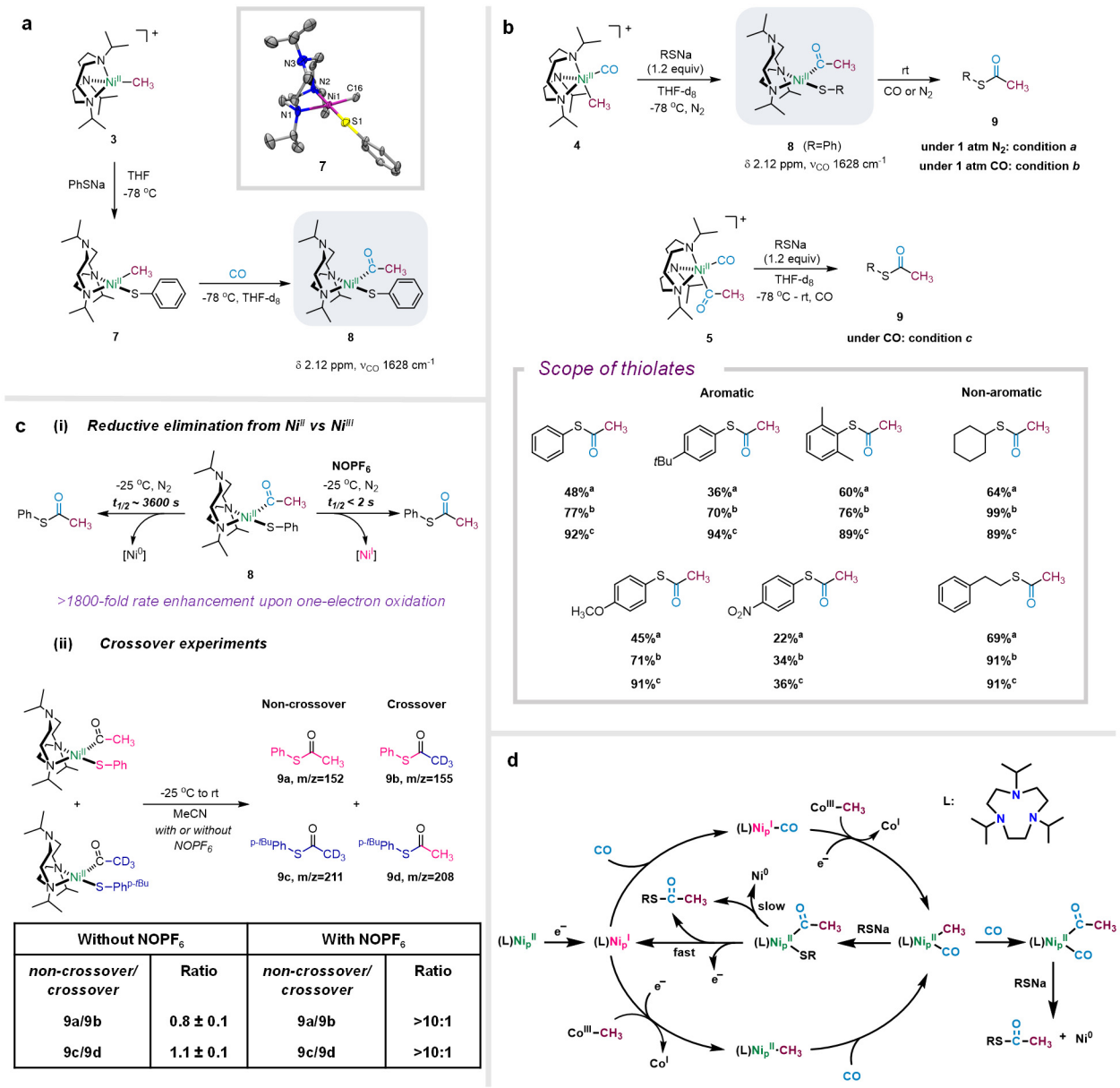

Without $NOPF_6$		With $NOPF_6$	
non-crossover/ crossover	Ratio	*non-crossover/ crossover*	Ratio
9a/9b	0.8 ± 0.1	9a/9b	>10:1
9c/9d	1.1 ± 0.1	9c/9d	>10:1

Fig. 4. Thiolysis of the model Ni complexes. (a) Synthesis of [(^{i}Pr$_3$tacn)Ni^{II}(CH$_3$)(SPh)] (**7**) and its reaction with CO to form [(^{i}Pr$_3$tacn)Ni^{II}(COCH$_3$)(SPh)] (**8**); ORTEP representation of **7** shown with ellipsoids drawn at 50% probability. **(b)** Generation of thioesters via the carbonylated complexes **4** and **5** under three different conditions; *condition a*: reaction of **4** with thiolates under 1 atm N_2; *condition b*: reaction of **4** with thiolates under 1 atm CO; *condition c*: reaction of **5** with thiolates under 1 atm CO. Yields of thioesters obtained from the corresponding aryl/alkyl thiolates under the three conditions are shown. **(c)** One-electron oxidation of **8** by $NOPF_6$ triggers a fast and

concerted reductive elimination: (i) 1800-fold rate enhancement for thioester formation via a transient Ni^{III} intermediate; (ii) crossover experiments between [($^{i}Pr_3$tacn)Ni^{II}($COCD_3$)(SPh)] and [($^{i}Pr_3$tacn)Ni^{II}($COCH_3$)($SPh^{p\text{-}tBu}$)] complexes suggest a concerted reductive elimination upon one-electron oxidation. **(d)** Summary of reactivity pathways for the ($^{i}Pr_3$tacn)Ni system described herein, which replicates all key steps in the proposed catalytic cycle of ACS.

Excitingly, a sequential synthetic strategy was employed, starting with the Ni^{II} precursor **1** that is activated *via* reduction to the Ni^{I} species **2**, followed by methylation with $Co^{III}(dmgBF_2)_2(CH_3)(py)$ in presence of a reductant ($CoCp_2$), carbonylation under 1 atm CO, and thiolysis with thiophenolate led to the formation of S-phenyl thioacetate in 61% yield (Table S4), while switching the order of addition of CO and methyl groups also led to the formation of the product in 34% yield (Table S5). To the best of our knowledge, this is the first example of thioester formation via reductive activation of a Ni^{II} center and independent addition of methyl, CO, and thiolate groups, thus reproducing all key steps of the catalytic cycle of ACS. Importantly, one-electron oxidation of the *in situ* generated **8** by $NOPF_6$ leads to a >1800-fold increase in the rate of thioester formation at -25˚C (Fig. 4c, i). Additionally, a negligible amount of crossover products are formed when a 1:1 mixture of [($^{i}Pr_3$tacn)Ni^{II}($COCD_3$)(SPh)] and [($^{i}Pr_3$tacn)Ni^{II}($COCH_3$)($SPh^{p\text{-}tBu}$)] are oxidized with $NOPF_6$ under an inert atmosphere (Fig. 4c, ii), strongly suggesting that one-electron oxidation drives a rapid, concerted reductive elimination reaction from a transient Ni^{III} intermediate (Fig. S77). The Ni^{I} species generated during this process is likely trapped by the NO product from $NOPF_6$ reduction, to form the previously reported [($^{i}Pr_3$tacn)Ni^{II}(NO)]$^{+}$ species (Fig. S77);[32] this one-electron oxidation during the thiolysis step can thus be a plausible pathway to regenerate the active catalyst as a Ni^{I} species, and thus close the reaction cycle and avoid the formation of dead-end Ni^{0} species. Importantly, in ACS a ferredoxin is proposed to act as an

electron shuttle that promotes electron transfer steps at both the activation and methylation steps, as well as at the thiolysis step to form the thioester product and regenerate the active Ni^{I} species.[50] Thus, based on these model studies we propose Nature may have devised a judicious way to channel an electron to oxidize the Ni^{II}(acetyl)(SCoA) intermediate to a Ni^{III} species that undergoes rapid reductive elimination to regenerate the active Ni^{I} species (Fig. 4d).

CONCLUSION

Described herein is a series of ($^{i}Pr_3$tacn)Ni complexes that are functional models of the Ni_p site in ACS and can replicate all key steps in the proposed catalytic cycle of ACS. In addition to isolating the elusive Ni^{II}(methyl)(CO) intermediate, we have demonstrated the chemical competence for both the methyl and CO groups being the first substrate to bind to the Ni^{I} center and provided insights into the nature of the various organometallic Ni intermediates and the plausible oxidation states of the Ni center during the catalytic mechanism of ACS. Kinetic studies suggest that binding of a second CO molecule to the Ni center can drive the CO migratory insertion step, suggesting that ACS might follow a similar process to promote rapid migratory insertion and the subsequent reductive elimination. The entry point into the catalytic cycle seems to be a Ni^{I} species that needs suitably timed electron transfers at the methylation and thiolysis steps to form the thioester product, likely via a Ni^{III} species that then regenerates the active Ni^{I} species in the process. Overall, we hope that the mechanistic insights obtained from these studies will enable the exploration of the various proposed enzymatic mechanisms, and that the experiments described herein will inspire new enzyme mechanistic studies to gain a better understanding of the function of ACS and ACDS.

METHODS

Synthesis of [(^{i}Pr$_3$tacn)Ni^{II}(CH$_3$)]PF$_6$ (3): In a N_2 filled glovebox, a 20 mL vial equipped with a magnetic stir bar was charged with [(^{i}Pr$_3$tacn)Ni^{II}(NCMe)$_2$](PF$_6$)$_2$ (200 mg, 1 equiv, 0.291 mmol) and 5 mL 2-MeTHF. A second 20 mL vial was charged with the bis(trimethylaluminum)-1,4-diazabicyclo[2.2.2]octane adduct, DABAL-Me$_3$ (41.1 mg, 0.55 equiv, 0.160 mmol) and dissolved in 5 mL 2-MeTHF. Both solutions were cooled to -35˚C and the solution of DABAL-Me$_3$ was added dropwise to the suspension of [(^{i}Pr$_3$tacn)Ni^{II}(NCMe)$_2$](PF$_6$)$_2$ in 2-MeTHF. The reaction mixture was allowed to warm to room temperature and stirred overnight. The reaction mixture was then filtered to separate a purple precipitate, which was extracted several times with THF to yield a purple solution. This resulting purple solution was concentrated under vacuum and precipitated by the addition of excess pentane to yield a purple solid (110 mg, 82% yield). Crystals suitable for X-ray diffraction were obtained from a concentrated solution of **3** in 2-MeTHF at -35˚C. ^{1}H NMR (CD$_3$CN, 500 MHz) δ (ppm) 10.85 (br), 62.74 (br) 87.14 (br). UV-Vis, MeCN: λ, nm (ε, M^{-1}cm^{-1}): 527 (28), 349 (364), 255 (2104). Evan's method: μ_{eff} = 2.883μ_B (MeCN). EA: calculated for C$_{16}$H$_{36}$F$_6$N$_3$NiP: C 40.53% H 7.65% N 8.86%; found: C 40.28% H 7.46% N 8.69%.

Synthesis of [(^{i}Pr$_3$tacn)Ni^{II}(CH$_3$)(CO)]PF$_6$ (4): A Schlenk tube was charged with **3** (60 mg, 0.126 mmol) in 4 mL CH_2Cl_2 under N_2 atmosphere. The tube was cooled to -78˚C and CO was bubbled into the reaction mixture for 1 min. The solution immediately changed color to orange. The reaction mixture was then freeze-pump-thawed 3 times to remove any residual CO. The solution was then concentrated under vacuum and precipitated by the addition of pentane. An orange solid was isolated (59 mg, 93% yield). Crystals suitable for X-ray diffraction were obtained by vapor diffusion of pentane into a THF solution of **4**.

^{1}H NMR (CD_2Cl_2, 500 MHz) δ (ppm) 3.20 (sept, 6.5 Hz, 3H), 3.01-2.99 (m, 6H), 2.68-2.66 (m, 6H), 1.44 (d, 6.5 Hz, 18H), 0.34 (s, 3H). ^{13}C NMR (CD_2Cl_2, 125 MHz) δ (ppm) 179.76, 59.24,

45.21, 19.22, 4.54. UV-Vis, CH_2Cl_2: λ, nm (ε, $M^{-1}cm^{-1}$): 450 (424), 286 (4745), 252 (8676). IR (ATR): 2006 cm^{-1} (Ni-**CO**). EA: calculated for $C_{17}H_{36}F_6N_3NiOP \cdot CH_2Cl_2$: C 36.83% H 6.52% N 7.16%; found: C 36.89% H 6.52% N 7.68%.

Synthesis of [(^{i}Pr$_3$tacn)Ni^{II}(COCH$_3$)(CO)]PF$_6$ (5): In a N_2 filled glovebox, **4** (22 mg, 0.044 mmol) was dissolved in 4 mL THF in a vial. The vial was sealed with a rubber septum, removed from the glovebox, and bubbled with CO for 10 mins to ensure CO saturation in the solution. The vial were then allowed to stand under the 1 atm CO overnight at room temperature. Following this, pentane was allowed to diffuse into this solution at -35˚C. Orange crystals (15 mg) of **5** were isolated in 64% yield. **5** is unstable under a nitrogen atmosphere and slowly deinserts CO to form **4**. Hence all NMRs for **5** were recorded under 1 atm CO. ^{1}H NMR (CD_2Cl_2, 500 MHz) δ (ppm) 3.34 (sept, 6.5 Hz, 3H), 2.96-2.95 (m, 6H), 2.62 (s, 3H), 2.57-2.56 (m, 6H), 1.44 (d, 6.5 Hz, 18H). ^{13}C NMR (CD_2Cl_2, 125 MHz) δ (ppm) 221.01, 184.15, 59.44, 45.21, 38.10, 18.36. UV-Vis, CH_2Cl_2: λ, nm (ε, $M^{-1}cm^{-1}$): 450 (437), 340 (2983), 286 (3862), 232 (5189). IR (ATR): 2024 cm^{-1} (Ni-**CO**), 1709 cm^{-1} (Ni-**CO**Me). EA: calculated for $C_{18}H_{36}F_6N_3NiO_2P$: C 40.78% H 6.84% N 7.93%; found: C 40.87% H 6.89% N 8.07%.

References

1 Ragsdale, S. W. in *Comprehensive Coordination Chemistry III* Vol. 8 (eds Edwin C. Constable, Gerard Parkin, & Lawrence Que Jr) 611-633 (Elsevier, 2021).

2 Kung, Y. & Drennan, C. L. in *The Biological Chemistry of Nickel* Vol. 1 (eds Deborah Zamble, Magdalena Rowińska-Żyrek, & Henryk Kozlowski) 121-148 (The Royal Society of Chemistry, 2017).

3 Can, M., Armstrong, F. A. & Ragsdale, S. W. Structure, Function, and Mechanism of the Nickel Metalloenzymes, CO Dehydrogenase, and Acetyl-CoA Synthase. *Chem. Rev.* **114**, 4149-4174 (2014).

4 Ragsdale, S. W. & Pierce, E. Acetogenesis and the Wood-Ljungdahl pathway of CO2 fixation. *Biochim. Biophys. Acta, Proteins Proteomics* **1784**, 1873-1898 (2008).

5 Lindahl, P. A. Acetyl-coenzyme A synthase: the case for a Ni-based mechanism of catalysis. *J. Biol. Inorg. Chem.* **9**, 516-524 (2004).

6 Appel, A. M. *et al.* Frontiers, Opportunities, and Challenges in Biochemical and Chemical Catalysis of CO2 Fixation. *Chem. Rev.* **113**, 6621-6658 (2013).
7 Kalck, P., Le Berre, C. & Serp, P. Recent advances in the methanol carbonylation reaction into acetic acid. *Coord. Chem. Rev.* **402**, 213078 (2020).
8 Yoo, C. *et al.* Nickel-catalyzed ester carbonylation promoted by imidazole-derived carbenes and salts. *Science* **382**, 815-820 (2023).
9 Gu, W. W., Gencic, S., Cramer, S. P. & Grahame, D. A. The A-cluster in subunit β of the acetyl-CoA decarbonylase/synthase complex from *Methanosarcina thermophila*: Ni and Fe K-Edge XANES and EXAFS analyses. *J. Am. Chem. Soc.* **125**, 15343-15351 (2003).
10 Gencic, S., Duin, E. C. & Grahame, D. A. Tight Coupling of Partial Reactions in the Acetyl-CoA Decarbonylase/Synthase (ACDS) Multienzyme Complex from Methanosarcina thermophila: Acetyl C-C Bond Fragmentation at the A Cluster Promoted by Protein Conformational Changes. *J. Biol. Chem.* **285**, 15450-15463 (2010).
11 Darnault, C. *et al.* Ni-Zn-[Fe-4-S-4] and Ni-Ni-[Fe-4-S-4] clusters in closed and open subunits of acetyl-CoA synthase/carbon monoxide dehydrogenase. *Nat. Struct. Mol. Biol.* **10**, 271-279 (2003).
12 Ragsdale, S. W. & Wood, H. G. Acetate Biosynthesis by Acetogenic Bacteria - Evidence That Carbon-Monoxide Dehydrogenase Is the Condensing Enzyme That Catalyzes the Final Steps of the Synthesis. *J. Biol. Chem.* **260**, 3970-3977 (1985).
13 Can, M. *et al.* Characterization of Methyl- and Acetyl-Ni Intermediates in Acetyl CoA Synthase Formed during Anaerobic CO2 and CO Fixation. *J. Am. Chem. Soc.* **145**, 13696-13708 (2023).
14 Stavropoulos, P., Muetterties, M. C., Carrie, M. & Holm, R. H. Structural and Reaction Chemistry of Nickel-Complexes in Relation to Carbon-Monoxide Dehydrogenase - a Reaction System Simulating Acetyl-Coenzyme-a Synthase Activity. *J. Am. Chem. Soc.* **113**, 8485-8492 (1991).
15 Horn, B., Limberg, C., Herwig, C. & Mebs, S. The Conversion of Nickel-Bound CO into an Acetyl Thioester: Organometallic Chemistry Relevant to the Acetyl Coenzyme A Synthase Active Site. *Angew. Chem., Int. Ed.* **50**, 12621-12625 (2011).
16 Yoo, C., Oh, S., Kim, J. & Lee, Y. Transmethylation of a four-coordinate nickel(I) monocarbonyl species with methyl iodide. *Chem. Sci.* **5**, 3853-3858 (2014).
17 Manesis, A. C., Yerbulekova, A., Shearer, J. & Shafaat, H. S. Thioester synthesis by a designed nickel enzyme models prebiotic energy conversion. *Proc. Natl. Acad. Sci. U. S. A.* **119**, e2123022119 (2022).
18 Doukov, T. I., Blasiak, L. C., Seravalli, J., Ragsdale, S. W. & Drennan, C. L. Xenon in and at the end of the tunnel of bifunctional carbon monoxide dehydrogenase/acetyl-CoA synthase. *Biochemistry* **47**, 3474-3483 (2008).
19 James, C. D., Wiley, S., Ragsdale, S. W. & Hoffman, B. M. 13C Electron Nuclear Double Resonance Spectroscopy Shows Acetyl-CoA Synthase Binds Two Substrate CO in Multiple Binding Modes and Reveals the Importance of a CO-Binding "Alcove". *J. Am. Chem. Soc.* **142**, 15362-15370 (2020).
20 Tan, X. S., Sewell, C., Yang, Q. W. & Lindahl, P. A. Reduction and methyl transfer kinetics of the α subunit from acetyl coenzyme A synthase. *J. Am. Chem. Soc.* **125**, 318-319 (2003).
21 Gencic, S., Duin, E. C. & Grahame, D. A. The two-electron reduced A cluster in acetyl-CoA synthase: Preparation, characteristics and mechanistic implications. *J. Inorg. Biochem.* **240**, 112098 (2023).

22 Seravalli, J. & Ragsdale, S. W. Pulse-chase studies of the synthesis of acetyl-CoA by carbon monoxide dehydrogenase/acetyl-CoA synthase - Evidence for a random mechanism of methyl and carbonyl addition. *J. Biol. Chem.* **283**, 8384-8394 (2008).
23 Tucci, G. C. & Holm, R. H. Nickel-Mediated Formation of Thioesters from Bound Methyl, Thiols, and Carbon-Monoxide - a Possible Reaction Pathway of Acetyl-Coenzyme a Synthase Activity in Nickel-Containing Carbon-Monoxide Dehydrogenases. *J. Am. Chem. Soc.* **117**, 6489-6496 (1995).
24 Ram, M. S. & Riordan, C. G. Methyl Transfer from a Cobalt Complex to Ni(Tmc)(+) Yielding Ni(Tmc)Me(+) - a Model for Methylcobalamin Alkylation of Co Dehydrogenase. *J. Am. Chem. Soc.* **117**, 2365-2366 (1995).
25 Dougherty, W. G., Rangan, K., O'Hagan, M. J., Yap, G. P. A. & Riordan, C. G. Binuclear Complexes Containing a Methylnickel Moiety: Relevance to Organonickel Intermediates in Acetyl Coenzyme A Synthase Catalysis. *J. Am. Chem. Soc.* **130**, 13510-13511 (2008).
26 Ito, M., Kotera, M., Matsumoto, T. & Tatsumi, K. Dinuclear nickel complexes modeling the structure and function of the acetyl CoA synthase active site. *Proc. Natl. Acad. Sci. U. S. A.* **106**, 11862-11866 (2009).
27 Matsumoto, T., Ito, M., Kotera, M. & Tatsumi, K. A dinuclear nickel complex modeling of the Ni-d(II)-Ni-p(I) state of the active site of acetyl CoA synthase. *Dalton Trans.* **39**, 2995-2997 (2010).
28 Wilson, D. W. N. *et al.* Mixed Valence {Ni2+Ni1+} Clusters as Models of Acetyl Coenzyme A Synthase Intermediates. *J. Am. Chem. Soc.* **146**, 21034-21043 (2024).
29 Manesis, A. C., O'Connor, M. J., Schneider, C. R. & Shafaat, H. S. Multielectron Chemistry within a Model Nickel Metalloprotein: Mechanistic Implications for Acetyl-CoA Synthase. *J. Am. Chem. Soc.* **139**, 10328-10338 (2017).
30 Manesis, A. C. *et al.* A Biochemical Nickel(I) State Supports Nucleophilic Alkyl Addition: A Roadmap for Methyl Reactivity in Acetyl Coenzyme A Synthase. *Inorg. Chem.* **58**, 8969-8982 (2019).
31 Kisgeropoulos, E. C., Manesis, A. C. & Shafaat, H. S. Ligand Field Inversion as a Mechanism to Gate Bioorganometallic Reactivity: Investigating a Biochemical Model of Acetyl CoA Synthase Using Spectroscopy and Computation. *J. Am. Chem. Soc.* **143**, 849-867 (2021).
32 Griego, L., Woods, T. J. & Mirica, L. M. A five-coordinate Ni(I) complex supported by 1,4,7-triisopropyl-1,4,7-triazacyclononane. *Chem. Commun.* **58**, 7360-7363 (2022).
33 Can, M., Giles, L. J., Ragsdale, S. W. & Sarangi, R. X-ray Absorption Spectroscopy Reveals an Organometallic Ni–C Bond in the CO-Treated Form of Acetyl-CoA Synthase. *Biochemistry* **56**, 1248-1260 (2017).
34 Chmielowska, A., Lodowski, P. & Jaworska, M. Redox Potentials and Protonation of the A-Cluster from Acetyl-CoA Synthase. A Density Functional Theory Study. *J. Phys. Chem. A* **117**, 12484-12496 (2013).
35 Griego, L., Chae, J. B. & Mirica, L. M. A bulky 1,4,7-triazacyclononane and acetonitrile, a Goldilocks system for probing the role of Ni^{III} and Ni^{I} centers in cross-coupling catalysis. *Chem* **10**, 867-881 (2024).
36 Biswas, K., Prieto, O., Goldsmith, P. J. & Woodward, S. Remarkably stable (MeAl)•DABCO and stereoselective nickel-catalyzed AlR (R = Me, Et) additions to aldehydes. *Angew. Chem., Int. Ed.* **44**, 2232-2234 (2005).
37 Abubekerov, M., Gianetti, T. L., Kunishita, A. & Arnold, J. Synthesis and characterization of coordinatively unsaturated nickel(ii) and manganese(ii) alkyl complexes supported by the hydrotris(3-phenyl-5-methylpyrazolyl)borate (TpPh,Me) ligand. *Dalton Trans.* **42**, 10525-10532 (2013).

38 Seravalli, J., Brown, K. L. & Ragsdale, S. W. Acetyl coenzyme A synthesis from unnatural methylated corrinoids: Requirement for "base-off' coordination at cobalt. *J. Am. Chem. Soc.* **123**, 1786-1787 (2001).
39 Shultz, C. S., DeSimone, J. M. & Brookhart, M. Four- and five-coordinate CO insertion mechanisms in d(8)-nickel(III) complexes. *J. Am. Chem. Soc.* **123**, 9172-9173 (2001).
40 Shultz, C. S., DeSimone, J. M. & Brookhart, M. Cationic four- and five-coordinate nickel(II) complexes: Insights into the nickel(II)-catalyzed copolymerization of ethylene and carbon monoxide. *Organometallics* **20**, 16-18 (2001).
41 Tan, X. S., Surovtsev, I. V. & Lindahl, P. A. Kinetics of CO insertion and acetyl group transfer steps, and a model of the acetyl-CoA synthase catalytic mechanism. *J. Am. Chem. Soc.* **128**, 12331-12338 (2006).
42 Wiley, S. *et al.* An alcove at the acetyl-CoA synthase nickel active site is required for productive substrate CO binding and anaerobic carbon fixation. *J. Biol. Chem.* **300**, 107503 (2024).
43 Ragsdale, S. W., Wood, H. G. & Antholine, W. E. Evidence That an Iron-Nickel Carbon Complex Is Formed by Reaction of Co with the Co Dehydrogenase from Clostridium-Thermoaceticum. *Proc. Natl. Acad. Sci. U. S. A.* **82**, 6811-6814 (1985).
44 Cohen, S. E. *et al.* Crystallographic Characterization of the Carbonylated A-Cluster in Carbon Monoxide Dehydrogenase/Acetyl-CoA Synthase. *ACS Catal.* **10**, 9741-9746 (2020).
45 Seravalli, J., Kumar, M. & Ragsdale, S. W. Rapid kinetic studies of acetyl-CoA synthesis: Evidence supporting the catalytic intermediacy of a paramagnetic NiFeC species in the autotrophic Wood-Ljungdahl pathway. *Biochemistry* **41**, 1807-1819 (2002).
46 Gencic, S., Kelly, K., Ghebreamlak, S., Duin, E. C. & Grahame, D. A. Different Modes of Carbon Monoxide Binding to Acetyl-CoA Synthase and the Role of a Conserved Phenylalanine in the Coordination Environment of Nickel. *Biochemistry* **52**, 1705-1716 (2013).
47 Kumar, M. & Ragsdale, S. W. Characterization of the Co Binding-Site of Carbon-Monoxide Dehydrogenase from Clostridium-Thermoaceticum by Infrared-Spectroscopy. *J. Am. Chem. Soc.* **114**, 8713-8715 (1992).
48 Webster, C. E., Darensbourg, M. Y., Lindahl, P. A. & Hall, M. B. Structures and energetics of models for the active site of acetyl-coenzyme a synthase: Role of distal and proximal metals in catalysis. *J. Am. Chem. Soc.* **126**, 3410-3411 (2004).
49 Ariyananda, P. W. G., Kieber-Emmons, M. T., Yap, G. P. A. & Riordan, C. G. Synthetic analogs for evaluating the influence of N-H center dot center dot center dot S hydrogen bonds on the formation of thioester in acetyl coenzyme a synthase. *Dalton Trans.*, 4359-4369 (2009).
50 Bender, G. & Ragsdale, S. W. Evidence That Ferredoxin Interfaces with an Internal Redox Shuttle in Acetyl-CoA Synthase during Reductive Activation and Catalysis. *Biochemistry* **50**, 276-286 (2011).

Data availability:

CCDC numbers 2376140-2376143 contain the supplementary crystallographic data for this paper. These data can be obtained free of charge via www.ccdc.cam.ac.uk/data_request/cif, or by emailing data_request@ccdc.cam.ac.uk, or by contacting The Cambridge Crystallographic Data

Centre, 12 Union Road, Cambridge CB2 1EZ, UK; fax: +44 1223 336033. All other experimental, spectroscopic characterization, and X-ray crystallographic data are included in the supplementary materials.

Acknowledgments:

We thank the National Science Foundation (CHE 2155160 to L.M.M.) for support. We thank all the research facilities in the School of Chemical Sciences at the University of Illinois Urbana-Champaign for their help. We also thank Dr. Toby J. Woods for assistance with the data collection for determining the solid-state structures, and Sagnik Chakrabarti for helpful discussions related to this project.

Author contributions:

L.M.M., S.N. and L.G. conceived the overall project. S.N. and L.M.M. conceived and designed the experiments and computations. S.N. and L.G. carried out the experimental work. S.N. analyzed the data. S.N. and L.M.M. wrote the manuscript. L.M.M. directed the project.

Competing Financial interests:

The authors declare no competing financial interests.

Additional Information:

Supplementary information including full details of synthesis and characterization of new compounds, mechanistic experiments, catalysis, X-Ray crystallographic data, and DFT calculations is available for this paper.

Correspondence and requests for materials should be addressed to Liviu M. Mirica.